CERN
CH1211 Geneva 23
Switzerland

EN Engineering Department

EDMS NO.	REV.	VALIDITY
1724436	1.0	released

REFERENCE
R. Piccin (IO)

Date: 07/10/2016

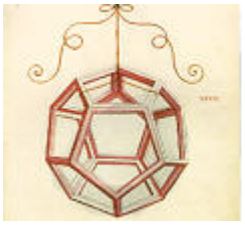

MME Mechanical & Materials Engineering

EN/MME MATERIALS & METROLOGY

Metallurgy Report

Analysis of ITER Axial Insulation Break (IBDH251)

DOCUMENT PREPARED BY:	DOCUMENT CHECKED BY:	DOCUMENT APPROVED BY:
P. Fernandez Pison EN/MME /MM TESTS DONE BY: P. Fernandez Pison EN/MME/MM A. Rivière TE/VSC/SCC	I. Aviles EN/MME/MM	S. Sgobba – EN/MME/MM

Distribution list: A. Laurenti, R. Piccin, J-Y Journeaux, M. Su (ITER Organization)

TABLE OF CONTENTS

1. Introduction

Insulation breaks (IBs) are required in the liquid helium feed pipes for the ITER magnets to isolate the high voltage system from the helium supply system. They consist essentially of stainless steel tubes (fittings) overwrapped to an outer composite (composite B) and bonded to an inner composite tube (composite A) by each end of the stainless steel fittings. Sometimes Glass – Kapton – Glass (GKG) insulation layers are interleaved in the outer composite (see Figure 1).

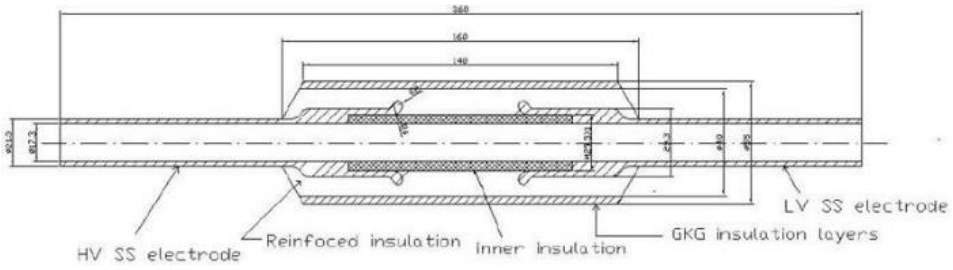

Figure 1: Schematic arrangement of an ITER Insulating Break (image obtained from IO).

One candidate break, 30 kV IB (Figure 2), was supplied to CERN on the 16th of September of 2016 for evaluation of the manufacturing quality. This insulation break is identified as IBDH251 as shown in Figure 3. It is important to note that it showed a small sign of damage in the outer surface in as-received state as can be observed in Figure 4.

Figure 2: Insulation break in as-received state.

Figure 3: Marking specifying the IB identification (IBDH251).

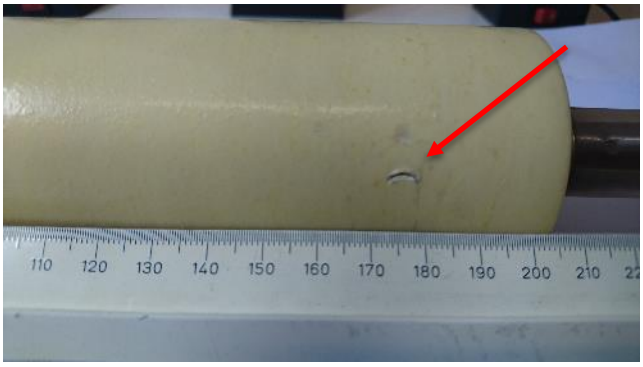

Figure 4: Imperfection in the outer surface of the IB.

1.1 Tests description

The test campaign which was agreed between CERN and IO is the following:

1. Sectioning the insulation break on a diametric plane, polishing and visual examination of one section through optical microscopy.
2. Dye penetrant testing.
3. Circumferential sectioning the non-polished section in order to extract the specimens and to perform a visual examination of the cross section.

For both composites of the insulation break, the following measurements were also done:

4. Measuring the relative density.
5. Measuring the volume fraction of voids, fibre and resin.
6. Measuring the glass transition temperature (T_g).
7. Measuring the fibre angle with respect to the longitudinal axis.

2. Results

2.1 Sectioning and inspection (axial)

In order to evaluate the manufacturing quality of the sample insulation break, it needs to be sectioned so that the internal structure can be examined.

The sample was slit along its axial centre line on a bench-mounted manual cutting machine as the one shown in Figure 5, obtaining a flat finish and an exploitable surface for further observation. Due to the nature of the piece to be cut (combination of metal and fibre glass reinforced epoxy resin), an Al_2O_3 based wheel capable of cutting materials up to HV 1000 was used, with a speed of 3000 rpm. The high-capacity recirculation system with pre-filter and decanter compartments ensures optimum lubrication and cooling of the piece by a multi-point spray.

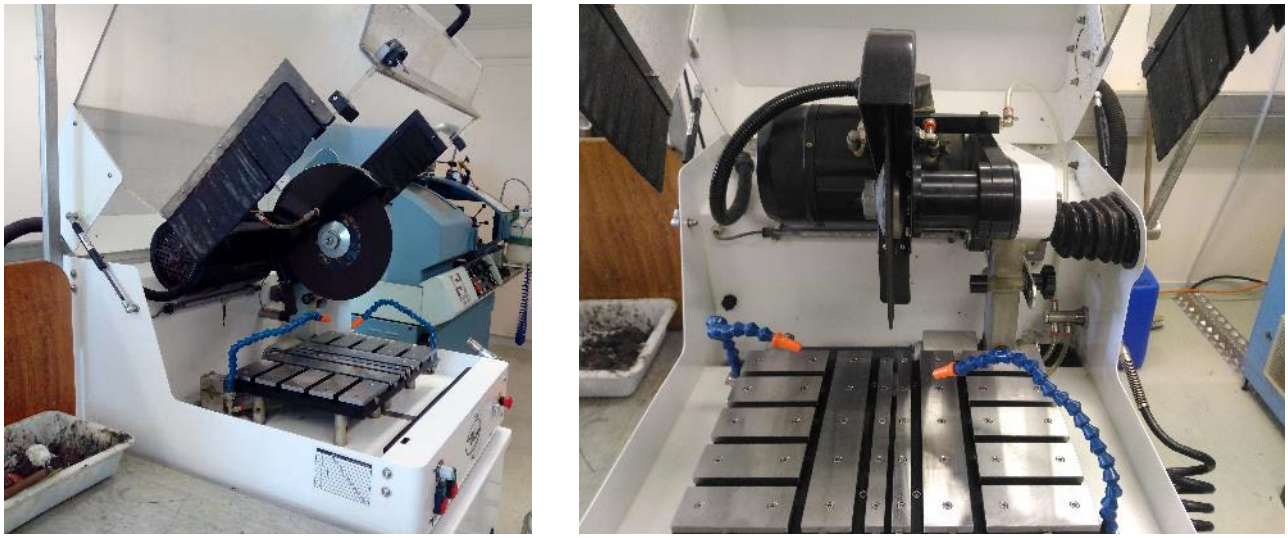

Figure 5: Bench-mounted manual cutting machine. Side view (left) and front view (right).

One half of the insulation break was inspected microscopically for any flaws in the structure. Since the cutting operation might have induced minor localized damage in the surface as the slightly burnt regions in the composites (dark regions close to the stainless steel fittings in Figure 6) one of the halves was manually polished to a final 1200 mesh size, what was considered sufficient to remove the affected regions and to reveal the relevant structure of the insulators (see Figure 7). However, as it can be observed in the micrographs, some slightly burnt regions still remain after the polishing.

Figure 6: Insulation break after axial sectioning. Cutting direction is shown for reference.

Figure 7 shows the location of the micrographs which were analysed in the insulation break (magnification: 50x). The two composites show good continuity between them (Field B, Figure 8). No big porosities are visible in any of the two composites. However, in some regions around the stainless steel fitting, some voids and cracks are observed (Field A, Figure 10; Field D, Figure 11; Field F, Figure 12). Moreover, The GKG insulation layers show some voids particularly concentrated towards the outer layer (Field C, Figure 12; Field E, Figure 13).

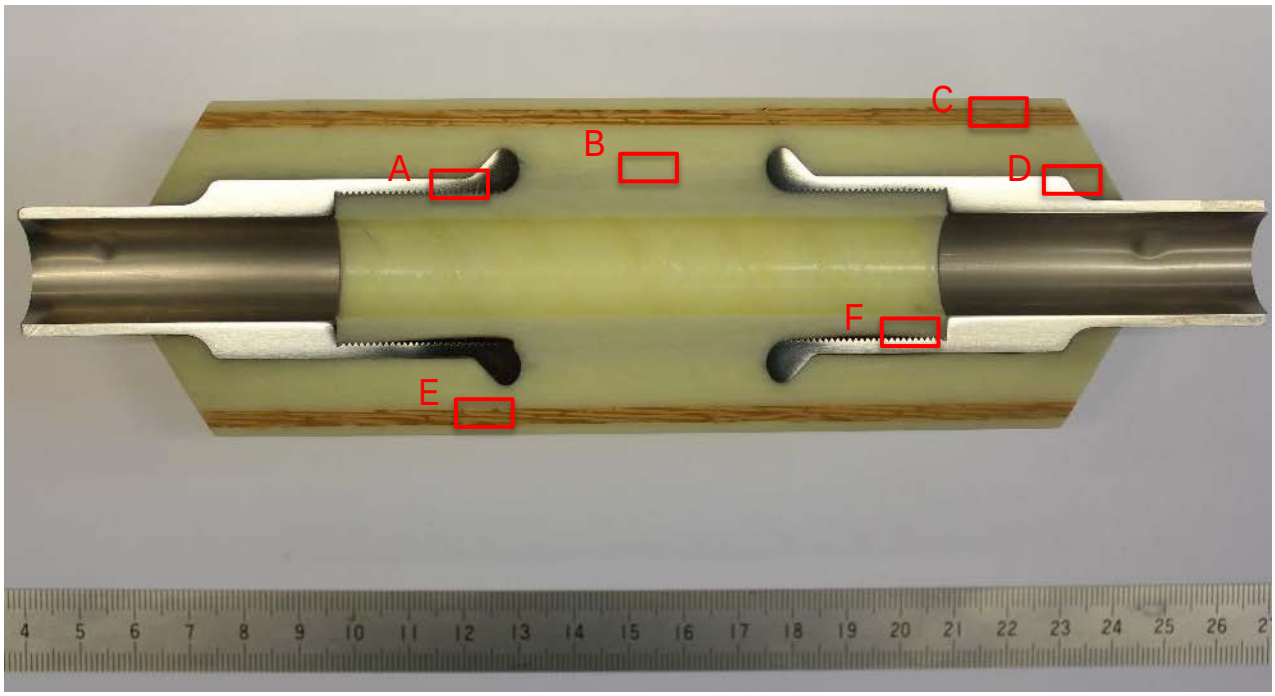

Figure 7: Half of the insulation break after manual polishing, indicating the fields of view used for showing specific features and their location.

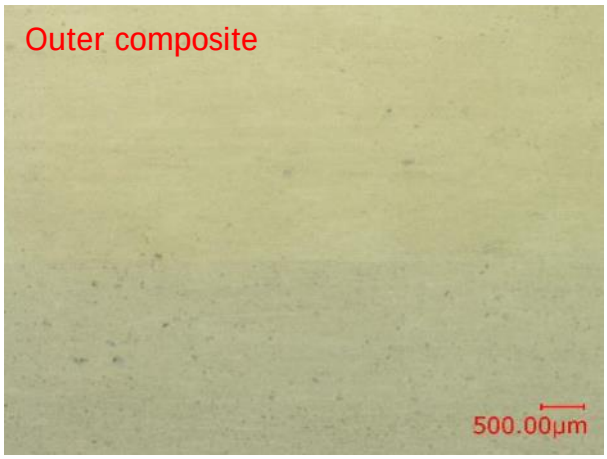

Figure 8: Interface between both composites (field of view B in Figure 7).

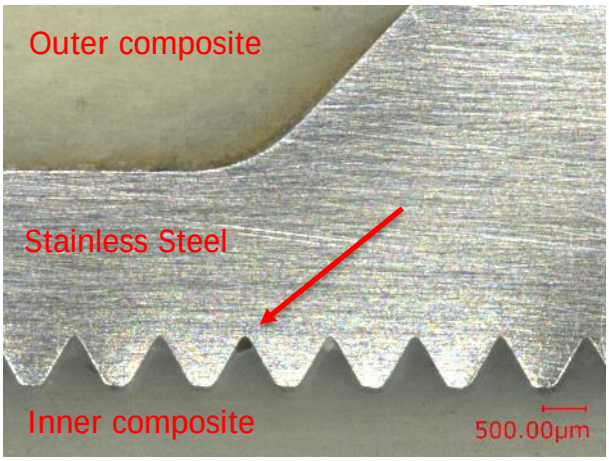

Figure 9: Void close to the stainless steel fitting region (field of view A in Figure 7).

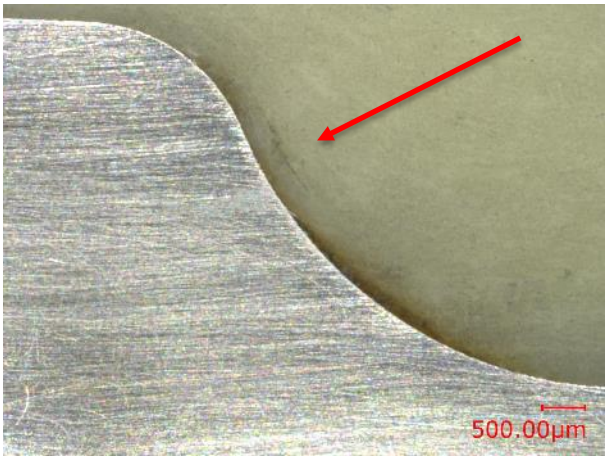

Figure 10: Cracks close to the stainless steel fitting region (field of view D in Figure 7).

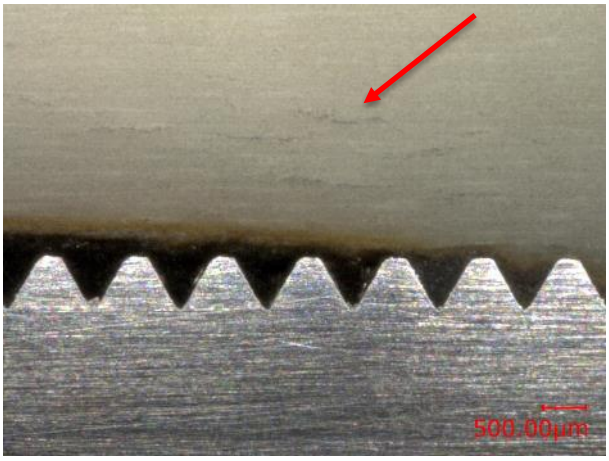

Figure 11: Cracks close to the stainless steel fitting region (field of view F in Figure 7).

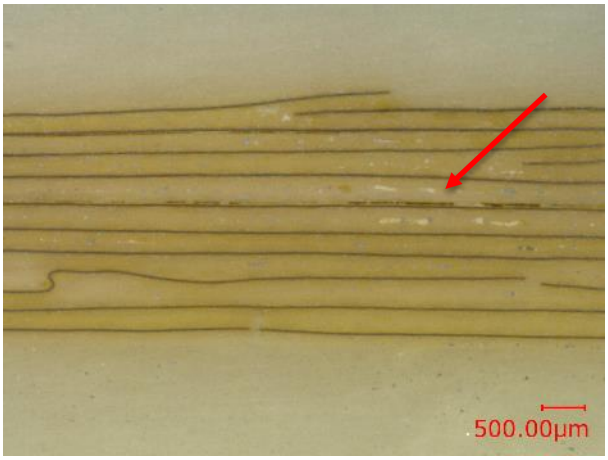

Figure 12: Voids in the GKG insulation layers (field of view C in Figure 7).

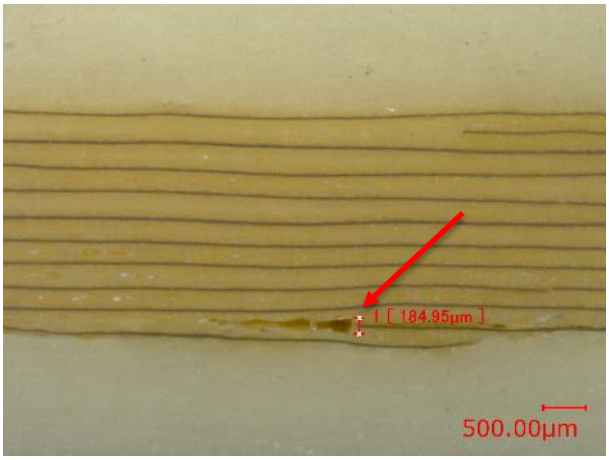

Figure 13: Voids in the GKG insulation layers (field of view E in Figure 7).

2.2 Dye penetrant testing

Dye penetrant examination was applied to both halves of the insulation break by Aline Piguiet, EN ISO 9712 PT level 2; Card n° BO2-012084. Type II (visible dye) method A (water washable) according to ASTM E1417 dye penetrant testing was carried out.

As it can be seen in Figure 14 and Figure 15, respectively, 5 minutes after the developer is applied, very pronounced linear indications are mainly observed in the stainless steel – to – composite interfaces and in the GKG insulation layers (also in the imperfection localized in the outer surface shown in Figure 4). The big amount of dye penetrant observed in some regions is a sign of a deep discontinuity associated to the respective indications.

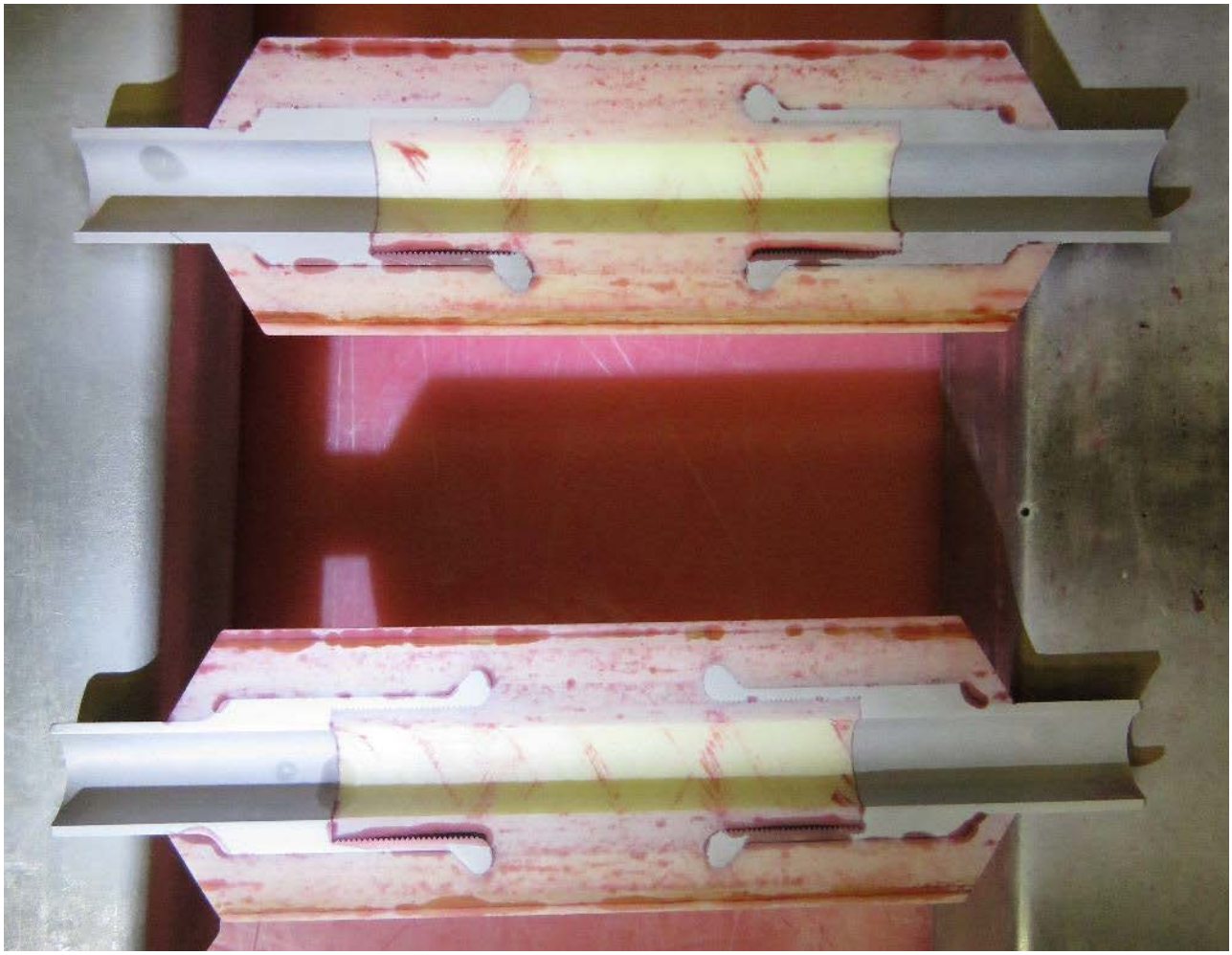

Figure 14: Internal surface of the insulation break after application of developer. Dwell time: 5 minutes.

Figure 15: Outer surface of the insulation break after application of developer. Dwell time: 5 minutes.

It is noteworthy that two longitudinal indications revealed by dye penetrant testing were not noticed during the micro-optical inspection (indications shown by arrows in Figure 16). It seems like the indications are deep but the exposed surface in the IB axial cross-section is small. In spite of that, the indications found by dye penetrant testing agree fairly well with the micro-optical observations (see Figure 16).

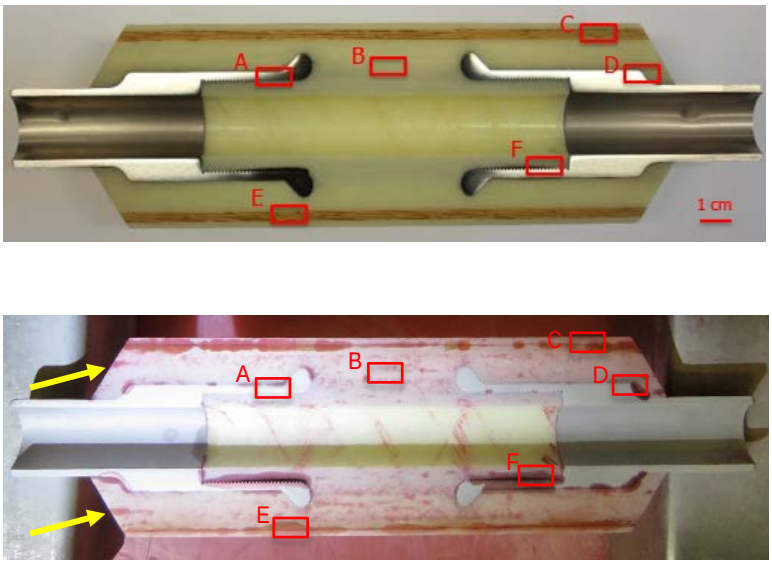

Field	Description
A	Void surrounding the metal area
B	Interface with good quality
C	GKG insulation layers with some voids.
D	Crack surrounding the metal area.
E	GKG insulation layers with some voids.
F	Cracks surrounding the metal area.

Figure 16: Comparison between the results obtained by the micro-optical analysis and the dye penetrant testing.

As indicated before, the cutting operation might have locally affected the external surfaces of the insulation breaks. Nevertheless, the intense indications observed after PT suggest deep discontinuities in the material that could not be induced by the cutting operation.

2.3 Sectioning and inspection (cross sectional)

2.3.1 Sample preparation

After the axial sectioning, penetrant testing and subsequent cleaning, the non-polished half of the insulation break was prepared to be used for the several measurements.

It was sectioned in three portions on a cutting wheel (Figure 5) as sketched in Figure 17: portion A was used for the cross sectional inspection, from portion B the inner composite was extracted, and from portion C the outer composite was extracted. Inner composite and outer composite from portions B and C, respectively, were used for measuring the relative density, for the calculation of the fibre content in the composite, for the estimation of the fibre angle and for measuring the glass transition temperature.

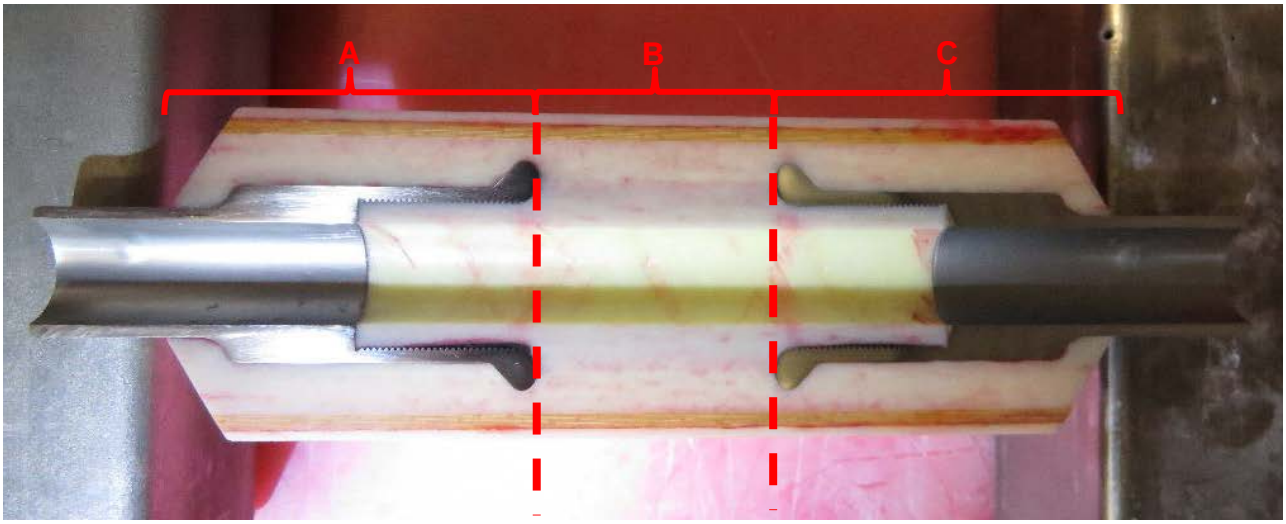

Figure 17: Three portions distinguished in each non-polished half of the insulation break.

Previous to the cross sectional cut, portions B and C were prepared: a lathe and a specific tooling designed to be able to turn the specimens were used to separate the outer composite from the inner composite in portion B and the GKG insulation layers from the outer composite. For this operation, a Weiler lathe was used (Figure 18) with a BN coated insert for the material removal (Figure 19). Figure 20 shows the preparation process.

Figure 18: Lathe for sample preparation.

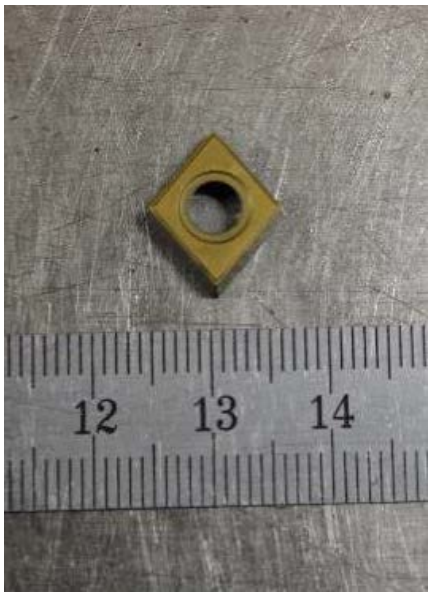

Figure 19: Insert used for material removal.

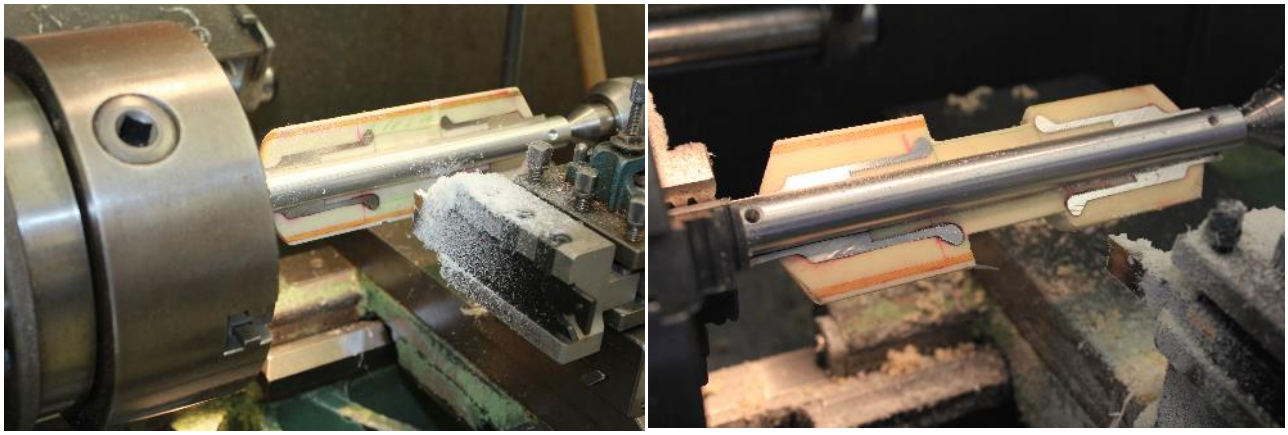

Figure 20: Preparation process before using the lathe to obtain the individual composites.

For the final preparation step, the inner composite and the stainless steel fitting was separated from the outer composite in portion C by gripping the metallic part and applying pressure to the outer composite (Figure 21).

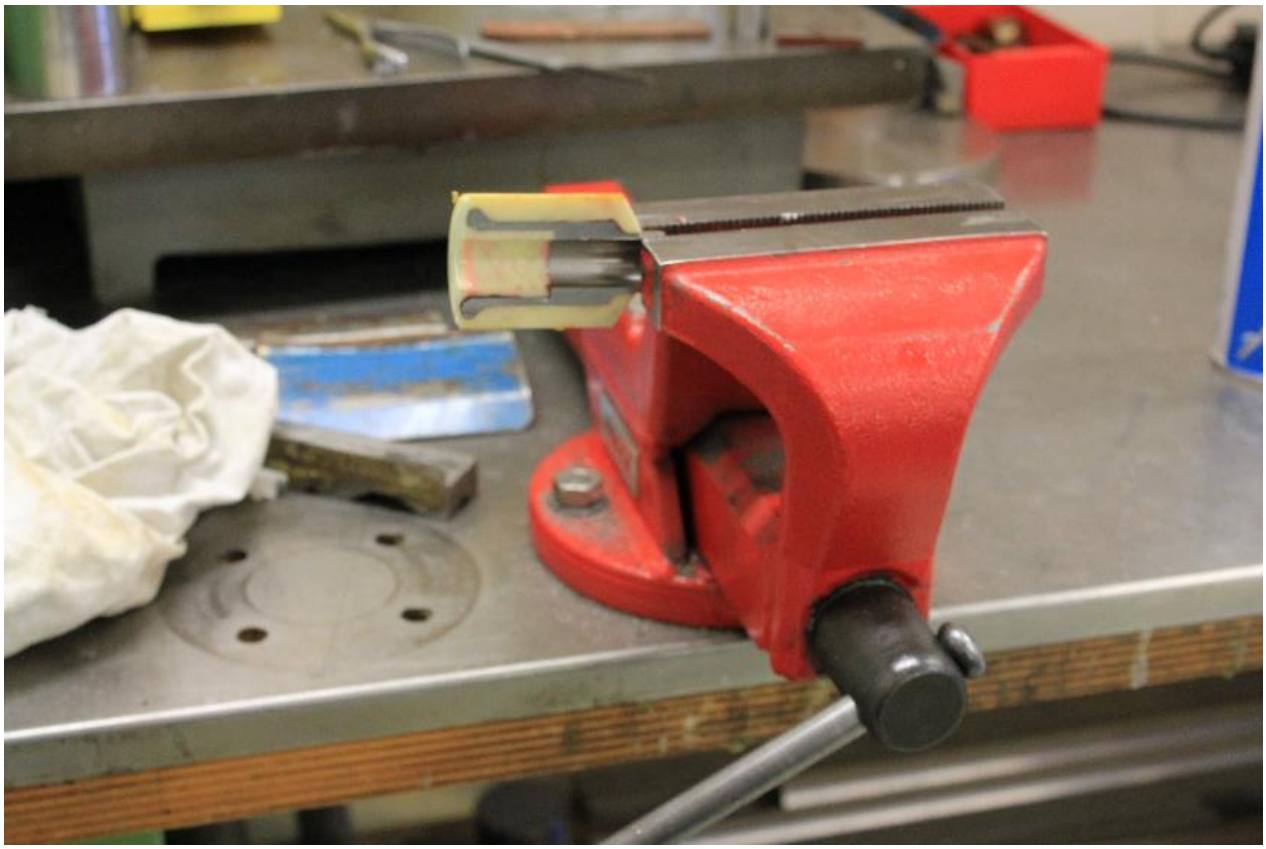

Figure 21: Separation of the inner composite - stainless steel fitting from the outer composite in portion C.

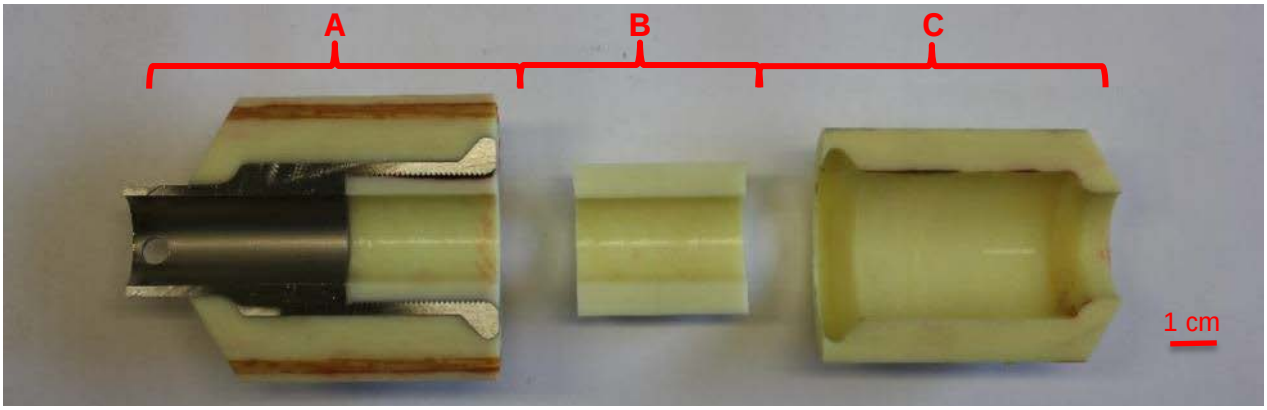

Figure 22: Insulation break sectioned into the three different portions.

2.3.2 Cross sectional inspection

The cross section of portion A of the insulation break was polished to a final 1200 mesh size, what is sufficient to reveal the relevant structure of the insulator.

As it can be seen in Figure 23, small linear indications are observed in the stainless steel – composite interface, and a long indication is observed in the last layer of the outer GKG insulation. Both cross sections were obtained in correspondence of major indications from PT performed in the axial plane (no additional PT has been performed for the cross sectional inspection). Consistently, in these positions, the cross sectional micro optical observations have confirmed indications present in the bulk.

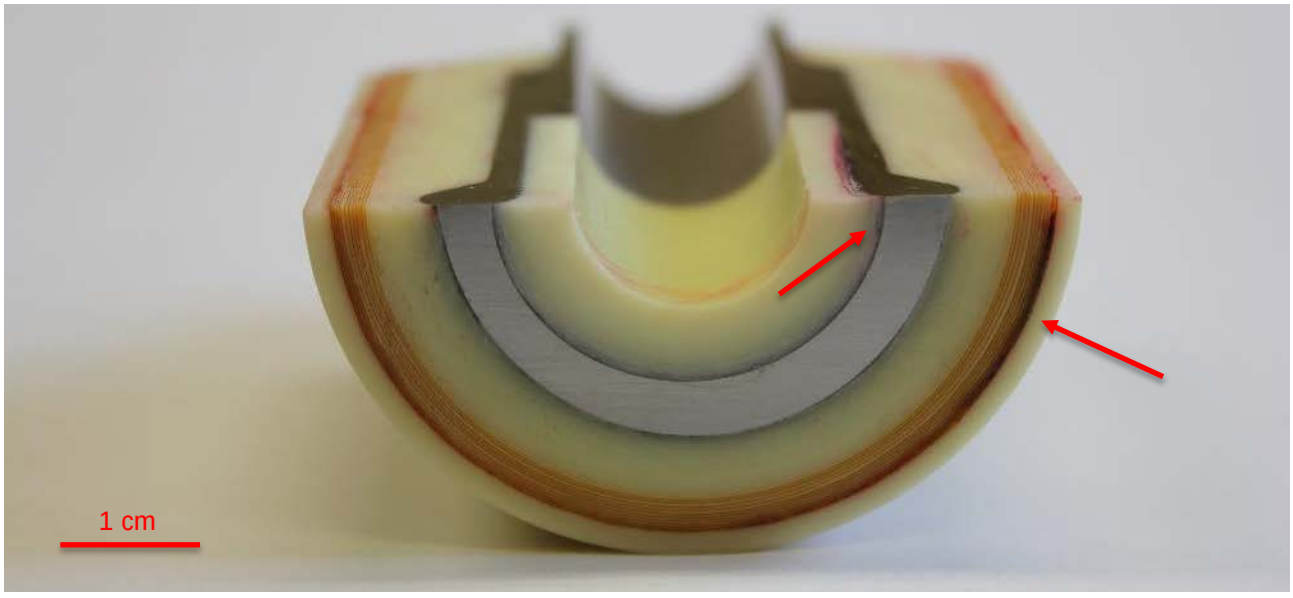

Figure 23: Cross sectional inspection of the insulation break. The arrows show the indications from PT located in: the stainless steel-composite interface and in the last layer of the GKG insulation layers.

2.4 Density

The measurement of the density of a composite material is a necessary step in determining the void content of the material. The measurement was made using Archimedes' principle, which is simple to perform and yields highly repeatable results. The calculation of the density was done according to ASTM D792, using pure ethanol as process fluid.

Taking into account that the insulation break is composed of 2 composites, an assessment of the density for each of them was performed. Two samples of approximately 5 g each (as required by the standard) for each composite were extracted from portions B and C (see image Figure 22) and measured three times each in order to ensure repeatable density values could be obtained. Previously, the samples were ultrasonically cleaned for 5 minutes, rinsed with demineralised water and dried in an oven at 80 ºC for two hours. For the weightings, a Sartorius analytical balance as the ones shown in Figure 24 was used.

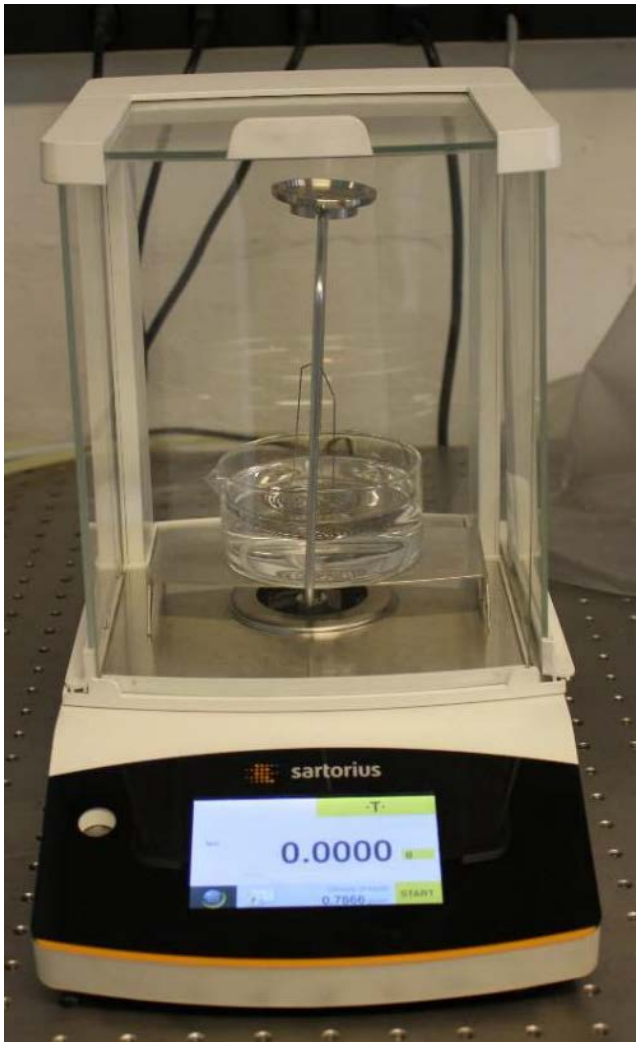

Figure 24: Analytical balance used for the density measurements.

The results of the densities are shown in Table 1:

Table 1: Summary table of the densities.

Sample		Density [g/cm^3]
Outer composite	Sample 1	1.84 ± 0.02
	Sample 2	
Inner composite	Sample 1	1.91 ± 0.00
	Sample 2	

2.5 Void fraction, % fibre and % resin

The assessment of the volume fraction of fibre, resin and void was performed according to ASTM D2584. The samples which were used for the determination of the density were weighted three times each in order to ensure repeatability of the values. They were subsequently fired in a furnace at 550 ºC for approximately 2 hours. They were cooled inside the furnace by natural convection and weighted again as soon as they reached room temperature (see Figure 25 and Figure 26).

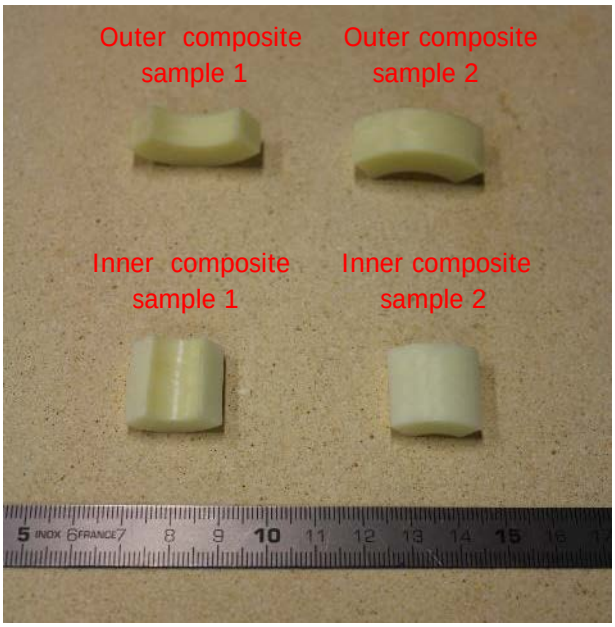

Figure 25: Samples before combustion.

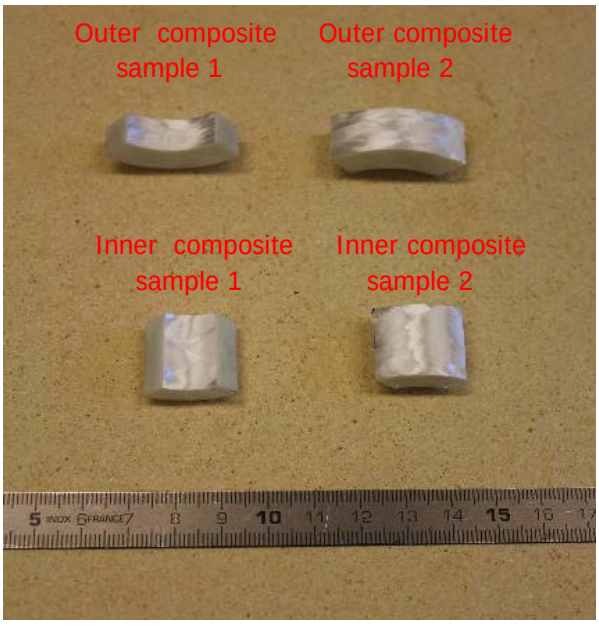

Figure 26: Samples after combustion.

The obtained results are summarised in Table 2, with the different volume fractions calculated as follows:

$$VF_f = \frac{M_f\,\rho_s}{M_s\,\rho_f}\,100\,; \qquad VF_r = \frac{M_r\,\rho_s}{M_s\,\rho_r}\,100; \qquad VF_v = 100 - (VF_f + VF_r);$$

Where:

M_s = Mass of unfired sample [g]

M_f = Mass of fired sample (mass of fibre) [g]

$M_r = M_s - M_f$ = Mass of resin in the sample [g]

ρ_s = Density of unfired sample [g cm^{-3}] (values taken from Table 1)

ρ_f = Density of fibre [g cm^{-3}] ($\rho_f = 2.65$ given by IO)

ρ_r = Density of resin [g cm^{-3}] ($\rho_r = 1.2$ given by IO)

VF_f = Volume fraction of fibre [%]

VF_r = Volume fraction of resin [%]

VF_v = Volume fraction of void [%]

Table 2: Summary of the void fraction, % fibre and % resin obtained by weighting and firing the samples previously used for density assessment

Sample		Unfired mass [g]	Fired mass [g]	vol % fibre	vol % resin	% void fraction
Outer composite	Sample 1	4.0	2.6	45.6 ± 1.5	52.2 ± 1.5	2.2 ± 0.0
	Sample 2	5.8	3.9			
Inner composite	Sample 1	4.1	2.9	50.6 ± 0.1	47.5 ± 0.2	1.9 ± 0.1
	Sample 2	4.0	2.8			

2.6 Glass transition temperature (T_g)

The evaluation of the glass transition temperature of each of the two composites (inner and outer) was done according to IEC 61006. For that purpose, small samples representative of each position were extracted (from portions B and C respectively) and delivered to the chemistry laboratory of CERN (TE/VSC). T_g was assessed via differential scanning calorimetry (DSC) using a SETARAM 131 calorimeter. 20 mg powder samples obtained by ball milling were warmed up with a ramp of 10ºC/min to a temperature of 200ºC under a nitrogen atmosphere. The process was repeated twice for each of the samples, with a forced convention cool down (50 mL/min of pure N_2) between the two measurements. Figure 27 and Figure 28 show the thermograms obtained for both composites together with a graphical calculation of T_g, performed according to IEC 61006.

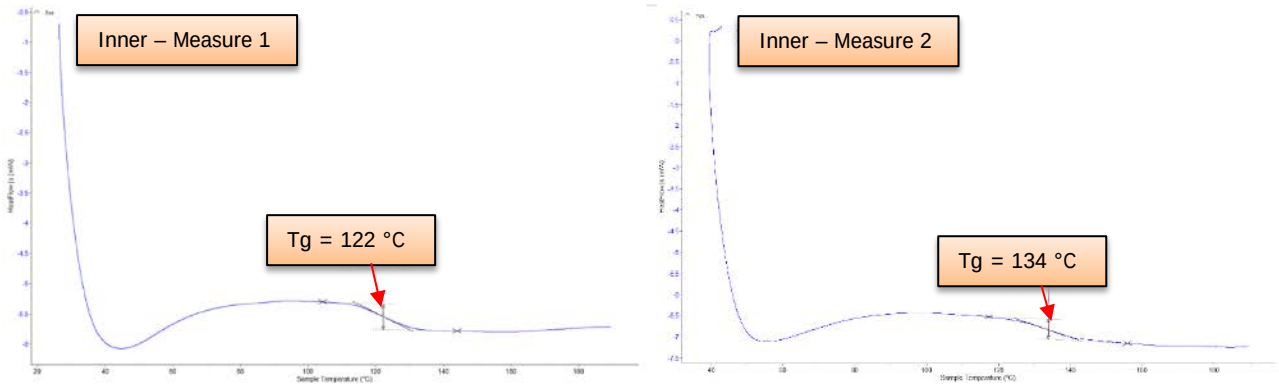

Figure 27: Thermograms for the inner composite for the calculation of Tg. On the left the first measure is observed and on the right, the second one.

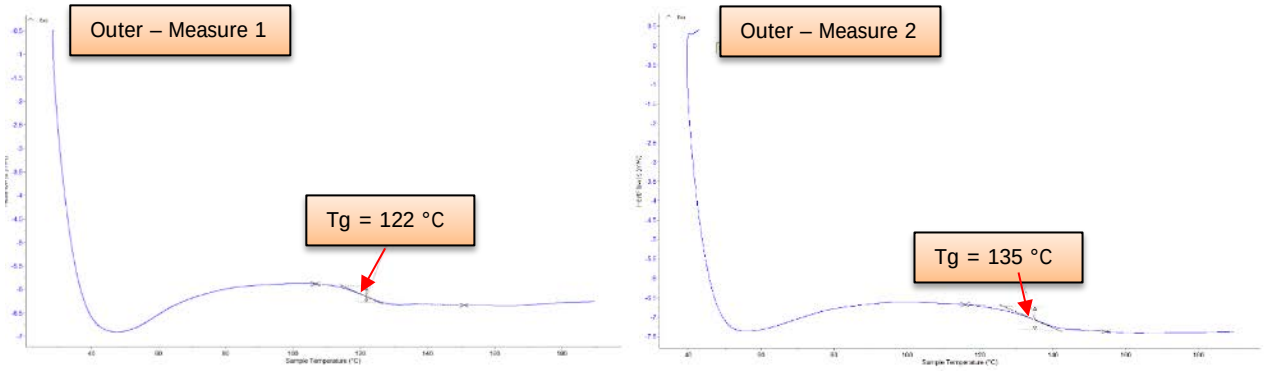

Figure 28: Thermograms for the outer composite for the calculation of Tg. On the left the first measure is observed and on the right, the second one.

The glass transition temperatures obtained for each of the composites for both insulation breaks are displayed in Table 3:

Table 3: Glass transition temperatures.

Sample	T_{g1} [° C]	T_{g2} [° C]
Outer composite	122	135
Inner composite	122	134

The first DSC scans show that for the first temperature ramp up, both composites display the same glass transition temperature (T_{g1}). For the second temperature ramp up, a rise in T_g for both composites is observed, which is suspected to be due to an incomplete polymerization.

2.7 Fibre angle

In order to estimate the fibre angle in the insulators, the samples previously used for density and void fraction assessment were used after combustion. The fired specimens were photographed with a KEYENCE digital microscope which allows us to take images with a large depth of field. Fibre angles were measured from the photographs (see Figure 29 as an example).

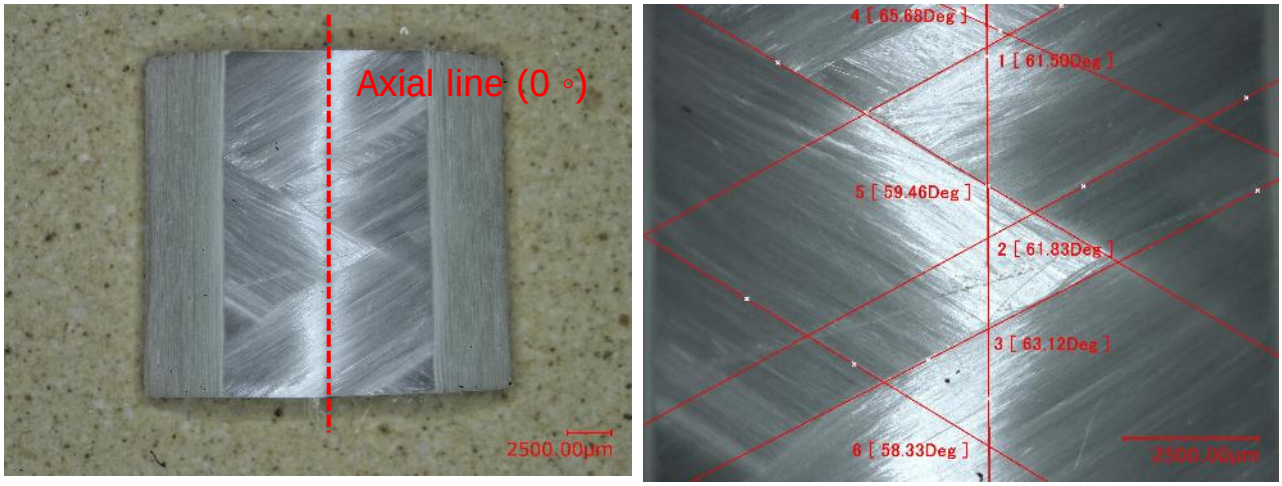

Figure 29: Fibre angle measurement. As an example, the sample 1 of the inner composite after firing is shown (left). Fibre angle with respect to the axial line of the insulation break (vertical red line) are observed (right).

Note that measuring the fibre angle on the curved surface introduces errors. Also, it is important to note that only the fibre angle from the visible layers can be measured due to the fact that pulling the specimens apart to examine underlying fibres can modify the orientation of the fibres, causing further errors. In order to have more statistics, for both composites, the internal and external surfaces were observed (see Figure 25 and Figure 26). Moreover, as it can be seen in Figure 29, 2 directions are observed for all of the composites, which are considered as equivalent taking into account that they are one perpendicular to the other with respect to the axial axis. The fibre angles measured from the photographs are shown in Table 4:

Table 4: Summary of the fibre angles measured for the different composites.

Sample	Average direction (wrt to axis) [°]
Outer composite	73.5 ± 4.4
Inner composite	60.8 ± 2.2

3. Conclusions

In view of the facts observed in the analyses, the interfaces of both insulator breaks, in the observed diametric and cross-sectional planes, have an important number of cracks and discontinuities, being of a considerable depth for most of the cases. Moreover, it exists a clear correlation between the defects identified during the optical observations and the penetrant testing. It is important to note that the observations were done in a single cross section per each axial and radial direction. The most critical defects are observed around the stainless steel fittings, in the interface between the composites and the stainless steel. They are not forming a continuous network along the interfaces and therefore they do not jeopardize the leak tightness assembly. Another critical region of imperfections is the GKG insulation layers, which present a poorer state with respect to an equivalent IB (identified as DL09) previously analysed at CERN (EDMS no. 1678587).

The density of the composites was accurately calculated according to ASTM D792. The repeatability of the results is quite high, with a value of 1.87 ± 0.05 g / cm^3 for all the composites analysed. In comparison with the insulation break identified as DL09, previously analysed at CERN (EDMS no. 1678587), similar densities of the outer and the inner composite were obtained (1.88 ± 0.03 g/cm^3 in average).

The volume fraction of fibre and resin were calculated in a macroscopic way, in the same samples used for the density (samples of approximately 5 grams), according to ASTM D2584. In the analysis, the volume fraction of void is 2.1 ± 0.2 %. Comparing the results with the values obtained for the insulation break identified as DL09, previously analysed at CERN (EDMS no. 1678587), a slightly lower value was obtained for the volume fraction of void (1.8 ± 0.1 %).

The orientation of the fibres was also determined with a reasonable accuracy via optical microscopy as required in the technical specification. It resulted in 60.8 ± 2.2 ^{0} for the inner composite and 73.5 ± 4.4 ^{0} for the outer, which fairly agrees with the ones obtained for the insulation break identified as DL09, previously analysed at CERN (EDMS no. 1678587), where an angle of 60.6 ± 3.3 ^{0} and 70 ± 3.1 ^{0} were observed for the outer and inner composite respectively.

Additionally, the glass transition temperature was calculated for both composites of the insulation breaks. A polymerization problem has been pinpointed, measuring an unstable T_g after the first heat treatment (T_{g1} =122 ^{0}C and T_{g2} =134.5 ^{0}C ± 0.5 ^{0}C). The same behaviour was observed for the insulation break identified as DL09, previously analysed at CERN (EDMS no. 1678587). For that case, the first measurement of the glass transition temperature for the outer composite was slightly lower (T_{g1} = 114 ^{0}C) than for the inner composite

(T_{g1} = 124 ^{0}C) the latter being similar to the value obtained in the actual insulation break. While after the second DSC scan, the glass transition temperature of both previously and presently investigated composites reaches similar values (T_{g2} = 130 ± 1 ^{0}C versus T_{g2} =134.5 ^{0}C ± 0.5 ^{0}C for the present one).